

Preparation and Motion Study of Magnetically Driven Micro Soft Robot Mimicking the Cownose Ray

Jiaqing Chang¹ * , Song Gao¹, Chaowei Dong¹, zhaobang Li¹, Yang Liu¹

(1. School of Mechanical and Electric Engineering, Guangzhou University, Guangzhou 510006, China)

Abstract: In narrow, unstructured underwater environments such as environmental monitoring and minimally invasive medical procedures, micro soft robots exhibit unique advantages due to their flexible movement capabilities and small size. At the same time, applying bionic technology to the structural design of micro soft robots can significantly improve their swimming performance. However, limited by their miniaturization, these robots are difficult to power internally and usually adopt a wireless power supply method. This study designs and fabricates a magnetically responsive, cownose ray-inspired micro soft robot based on the swimming principle of the cownose ray. The robot is made of a certain proportion of neodymium-iron-boron (NdFeB) and polydimethylsiloxane (PDMS). Then, a three-dimensional Helmholtz coil is used to generate an oscillating harmonic magnetic field to conduct swimming experiments on the robot, exploring the influence of magnetic field parameters on the robot's swimming performance. The experimental results show that the swimming speed is the fastest at $B = 5$ mT and $f = 11$ Hz, reaching 5.25 mm/s, which is about 0.5 body lengths per second. In addition, by adjusting the current direction and frequency of the coil, the robot can perform different swimming modes such as straight swimming, turning swimming, and directional swimming. By employing a stepwise adjustment method, the impact of response errors on the robot's trajectory can be effectively reduced. This study demonstrates a method for magnetically driven micro soft robots, laying a foundation for the application of wireless-driven robots in underwater narrow spaces.

Key words: micro soft robot; magnetic field driving; bionic technology; cownose ray; three-dimensional Helmholtz coil.

1 Introduction

In recent years, with the continuous development of robotic technology, micro soft robots are constantly overcoming the limitations of traditional rigid robots in terms of structure, adaptability, and movement patterns. As a cutting-edge product at the intersection of advanced materials and robotics, micro soft robots demonstrate significant application potential in fields such as biomedicine, environmental monitoring, and operations in confined spaces due to their miniaturized structure and rapid response capabilities, becoming a research hotspot for many scholars [1]. To further optimize the structure and movement methods of robots and achieve precise control over their movements, technical means based on bionic principles are typically used to design micro robots. By studying the structure and function of biological organisms in nature, their characteristics and movement patterns are referenced and applied to the structural design of micro robots, thereby better executing various work tasks. Examples include bionic insect-like micro robots [2-4], crawling bionic robots [5-7], fish-like bionic robots [8, 9], and tadpole-like bionic robots [10]. The propulsion mechanisms of fish in the ocean exhibit extremely high energy efficiency and maneuverability; by mimicking various fish species, the movement performance of underwater micro soft robots can be greatly enhanced. The swimming propulsion methods of fish can mainly be divided into two categories: Body-Caudal Fin (BCF) swimming and Median/Paired Fin (MPF) swimming [11,12]. The former is a typical characteristic of most fish, primarily generating thrust through axial oscillations of the fish body or periodic movements of the caudal fin; the latter generates traveling waves through the deformation of the pectoral fins, producing thrust from the reaction force of the water. BCF swimmers are known for their high-speed cruising and explosive acceleration, while MPF movement has advantages in maneuverability and stability [11,12]. The cownose ray, as a typical representative of BCF swimming, possesses excellent maneuverability and

efficient movement performance due to its unique wing-like structure and undulating motion. By mimicking the biological characteristics and movement mechanisms of the cownose ray, the efficient underwater propulsion capability of micro soft robots can be improved, as well as their ability to adapt to complex environments [13, 14].

The outstanding swimming ability of the cownose ray mainly comes from the deformation movement of its pectoral fins. To replicate this deformation, researchers have traditionally used linkage structures to achieve this motion. Chu Y et al. [15] proposed a bionic pectoral fin propulsion scheme for the cownose ray based on a six-bar mechanism, simulating the wave-like motion of the cownose ray's pectoral fins from head to tail by axially stacking two six-bar mechanisms of the same scaled size and setting a phase difference, demonstrating excellent underwater movement capabilities. However, it relies on external power sources and control cables, limiting autonomy and endurance. Similar studies include a bionic cownose ray robot designed by Wu J et al. [13], which uses a three-stage differential linkage mechanism to drive the pectoral fin oscillation, achieving stable underwater movement; Daili Zhang et al. [16] designed a bionic cownose ray robot that integrates gliding and flapping propulsion, achieving an organic combination of gliding propulsion and bionic pectoral fin flapping propulsion through a buoyancy/mass adjustment system and bionic pectoral fin driving mechanism. In these studies, most bionic cownose ray robots are rigid structures and large in size, leading to poor flexibility and limitations in narrow spaces. In contrast, bionic cownose ray robots designed with flexible materials exhibit higher environmental adaptability and safety. Giovanni B et al. [17] designed a bionic cownose ray robot that combines rigid and flexible structures, using a rigid body to house batteries, sensors, and other components, while the pectoral fins on both sides are driven by servomotors to achieve passive oscillatory propulsion. Zefeng Xu et al. [18] proposed a bionic dual-stable soft swimming robot that

can perform high-speed movement and multi-modal swimming. This robot uses prestressed composite materials to construct a dual-stable flapping structure, combined with a McKibben artificial muscle driving system, achieving multi-modal movements such as forward/backward swimming, turning, and underwater flipping through an asymmetric driving method of alternating pressurization/depressurization. Similar research includes a new type of bionic cownose ray soft electronic fish developed by Tiefeng Li's team [19], which integrates driving, power supply, and control into a fully soft structure, guiding the in-plane deformation of dielectric elastomers into wave-like movements of the fins to achieve efficient underwater propulsion. However, these types of robots, powered by external cables or built-in power sources, can lead to noticeable noise and limited endurance. To address these issues, it is necessary to introduce cable-free external power supply methods, such as light-driven [20], magnetic-driven [21], chemical-driven [22], and bio-driven [23]. Magnetic field drive, as a non-contact driving method, is widely used due to its strong penetration, precise control, and high biocompatibility [24]. According to the source of the magnetic field in the driving system, it can be divided into permanent magnet drive systems [25-28] and electromagnetic coil drive systems [29-31]. Permanent magnet drive systems utilize the inherent magnetic field of permanent magnets to drive robots without the need for external power, offering advantages such as simple structure, low energy consumption, and stable operation [32]. However, the magnetic field generated by this method often requires external moving devices to adjust the spatial orientation of the permanent magnets and the distance to the controlled micro robot to control the magnetic field energy applied to the micro robot. The working principle of the electromagnetic coil drive system is that the coil generates a controllable magnetic field when energized, allowing for regulation of the magnetic field by adjusting current and voltage, and combining multiple coils can also produce rotating and oscillating

magnetic fields. Using electromagnetic coils to generate magnetic fields for wirelessly driving micro robots is currently one of the most popular driving methods. Magnetic-driven micro soft robots are usually made of magnetic materials combined with flexible rubber. For example, the team at the Max Planck Institute for Intelligent Systems in Germany [33] designed a millimeter-scale magnetoelastic micro soft robot based on silicone-neodymium-boron composite materials, achieving multi-modal movement through magnetic field programming and demonstrating excellent autonomous movement capabilities in various media. Similarly, Chenyang Huang et al. [34] developed a magnetic-controlled soft micro robot inspired by the morphology of zebrafish using Ecoflex silicone and neodymium-boron, endowing the robot with a sinusoidal magnetic distribution through directional magnetization, achieving synchronized bionic oscillatory motion under the application of an oscillating magnetic field driven by a three-axis Helmholtz coil. Additionally, Venkiteswaran et al. [35] designed four different magnetically driven soft robots using neodymium-iron-boron and silicone rubber composites, controlled by an oscillating magnetic field generated by six coil arrays, achieving smooth movement on uneven surfaces. However, directly applying these modes to mimic the core motion characteristics of large-scale flexible flapping of the cownose ray still faces significant challenges: it is necessary to endow soft materials with sufficient magnetic responsiveness to produce large amplitude, periodic deformations, while ensuring coordination and high efficiency of actions in fluid, and integrating multiple movement modes such as propulsion, turning, and posture adjustment under a single magnetic field control. Therefore, in-depth research and construction of a magnetic-driven strategy capable of reproducing the core motion characteristics of the cownose ray, and systematically revealing its motion mechanics, is of great scientific significance and application value for the development of a new generation of high-performance, fully wireless, bionic underwater

micro soft robots.

This paper starts from the biomimetic propulsion mechanism of the cow-nose ray and integrates the principle of magnetic drive to design and fabricate a cownose ray soft robot with magnetic response characteristics that mimics the cow-nose ray, and studies its motion performance. Firstly, based on the principle of bionics, the overall structural model of the cow-nose ray mimicking cownose soft robot is established, referring to the biological characteristics and swimming characteristics of the cow-nose ray. The magnetic response cownose soft robot is prepared by using a certain proportion of silicone and magnetic particles, and a swinging harmonic magnetic field drive system is built to study the deformation principle and swimming performance of the cow-nose ray mimicking cownose soft robot under the action of a magnetic field. The robot achieves multiple motion modes such as straight forward, backward, turning, and directional movement under magnetic field drive.

2 Design and Fabrication of a Micro Soft Robot Mimicking the cownose ray

2.1 Structural Design of a Micro Soft Robot

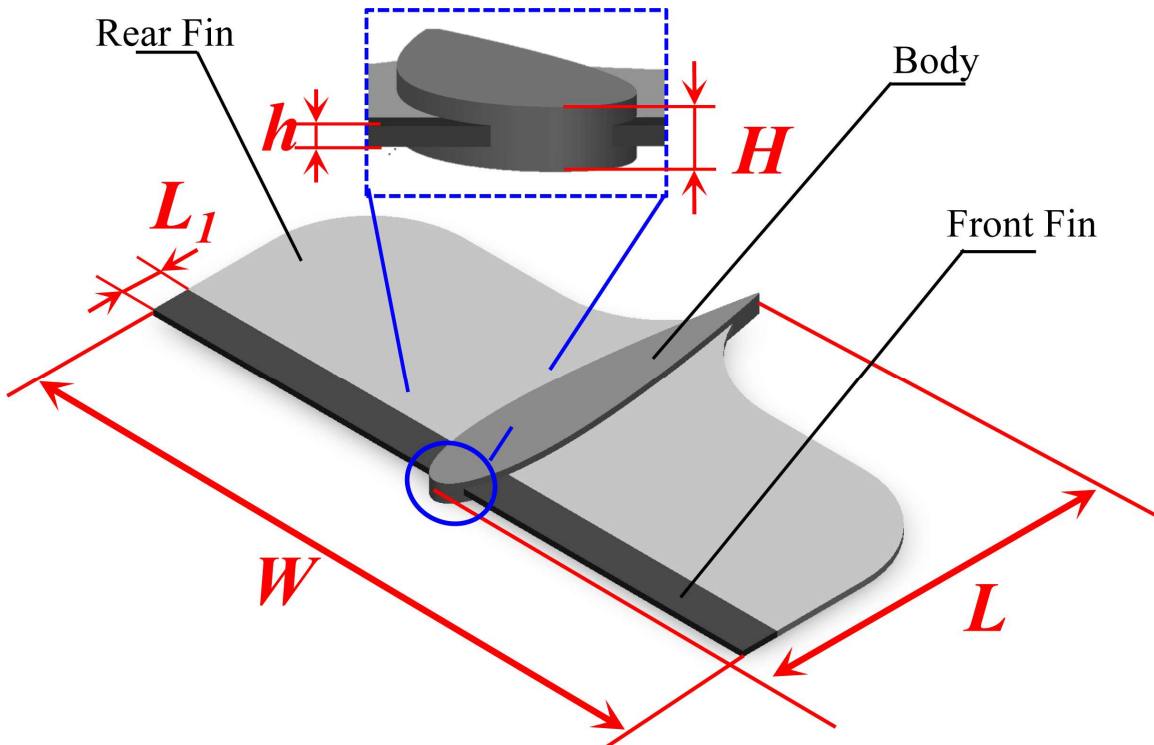


Figure 2-1 structure and dimensions diagram of the bionic cownose ray micro-soft.

Mimicking the cownose ray

The cow-nosed ray belongs to the order Myliobatiformes of the class Chondrichthyes. It has a flat, wide body with pectoral fins that almost cover the entire sides of its body. It primarily swims by flapping its wide pectoral fins up and down to generate thrust. According to existing research [36], during the swimming cycle of the cownose ray, the fin rays at the leading edge of the pectoral fin first move upward, followed sequentially by the rays in the middle and at the trailing edge, with a certain phase delay from front to back. Similarly, during the downward stroke of the pectoral fin, the fin rays at the leading edge also move downward first, followed in sequence by the middle and trailing edge rays, again with a certain phase delay. Based on this, the structure of the bio-inspired cownose ray robot we designed includes two main parts : the body and the pectoral fins, which are divided into the front fin and the rear fin according to the sequence of their oscillation start times.

As shown in Figure 2-1, the robot's front and rear fins are designed with a symmetrical distribution, and its body streamline adopts the NACA0018 four-digit airfoil, represented as NACA XYZZ, where X represents the relative curvature, that is, the ratio of maximum curvature to chord length; Y represents the position of maximum curvature, that is, the ratio of the position of maximum curvature to chord length, and ZZ represents the relative thickness, that is, the ratio of maximum thickness to chord length. In order to increase the contact area between the pectoral fins and the medium, providing better swimming performance, the pectoral fins are not designed to be completely triangular like those of a cownose ray, but instead have an increased leading edge width, forming a shape similar to a rectangle. The overall dimensions are length L of 11.34mm, width W of 20.56 mm, and height H of 1.5 mm, with the dimensions of other parts shown in Table 2-1.

Table 2-1 Dimensions of the Robotic cownose ray Micro Soft Robot

Part Name	Width (w)	Length (l)	Thickness (h)
Body	2mm	11.34mm	1.5mm
Front Fin	9.72mm	1 mm	0.12mm
Rear Fin	9.41mm	8.66 mm	0.12 mm

As the main power source in the bionic cownose ray robot, the swing performance of the pectoral fins is the key to ensuring the robot's efficient swimming performance. This puts certain requirements on the rigidity of the pectoral fin material. Appropriate rigidity affects whether the pectoral fins can overcome the fluid resistance of the medium and whether they have good flexibility. If the material is too rigid and lacks softness, it will cause the pectoral fins to bend not obviously during the swing process, affecting the robot's swimming; if the material is too soft, it may cause the fluid force generated by the pectoral fins to be insufficient to drive the robot to move. At present, the commonly used silicone materials for magnetically driven micro-soft robots are polydimethylsiloxane

(PDMS), high-elastic platinum-catalyzed silicone rubber (Smooth-On Ecoflex 00-10), and silica gel. as a magnetic response source, the pectoral fin needs to contain magnetic materials. Commonly used magnetic materials for making magnetic drive robot components include iron, cobalt, nickel, and their alloys, as well as some rare earth element alloys, such as neodymium iron boron (NdFeB), magnetite (Fe₃O₄), and hematite (Fe₂O₃). Magnetic materials need to be magnetized before being use, because unmagnetized magnetic materials have their internal magnetic moments in a disordered arrangement, the sum of all magnetic moment vectors is zero, and they appear non-magnetic externally[35]. Therefore, an external magnetic field needs to be applied to magnetize them. Coercivity and remanent magnetic induction intensity are key parameters that determine the stability of magnetic materials after magnetization. Through testing and comparison, we found that NdFeB has higher coercivity and remanent magnetic induction intensity. So, we selected NdFeB as the magnetic material to be mixed with silicone material for preparing micro soft robots. To select a suitable rigid material for the pectoral fin base, we conducted experiments by mixing polydimethylsiloxane (PDMS), highly elastic platinum-catalyzed silicone rubber (Smooth-On Ecoflex 00-10), and silica gel with NdFeB in equal proportions. Ultimately, the mixture of PDMS and magnetic particles showed the least bending deformation, so PDMS was chosen as the pectoral fin material for the micro soft robot. Then, the difference in magnetization intensity of the magneto-elastic composite materials containing different NdFeB contents was studied. As shown in Figure 2-2(a), by testing its magnetization curve and hysteresis loop, we found that with the increase of NdFeB content, the remanence and saturation magnetization intensity of the composite material gradually increased, but when the content reached 75wt%, the increase of NdFeB did not make the saturation magnetization intensity and remanence continue to increase significantly. The coercivity of the five magneto-elastic composite

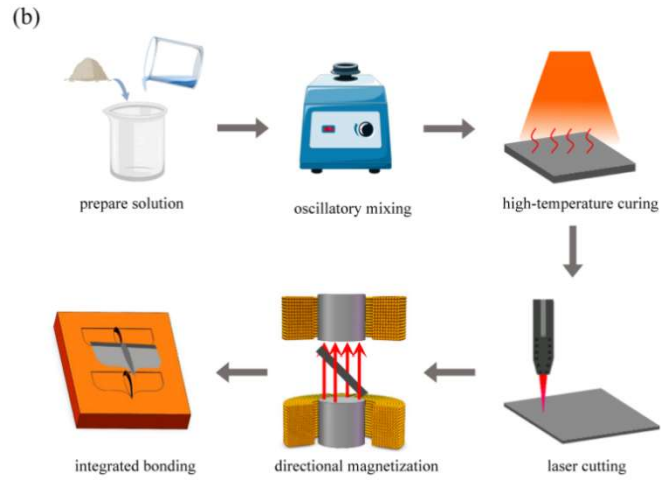
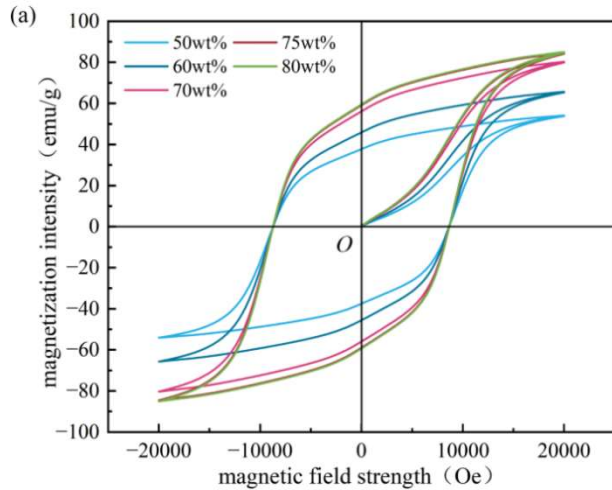


Figure 2-2 (a) Magnetization intensity and hysteresis loop of magneto-elastic composite materials with different NdFeB contents, (b) preparation process diagram of the bionic cownose ray micro-soft robot.

materials with different contents did not vary much, indicating that the magnitude of coercivity has no obvious relationship with the content of ferromagnetic material. Therefore, in the subsequent robot preparation, a magneto-elastic composite material containing 75wt% NdFeB was selected for production.

2.2 Fabrication of a Micro Soft Robot Mimicking the cownose ray

The preparation of the magnetically driven micro-soft robot mainly includes the following steps: mold printing, magneto-elastic composite solution preparation, laser cutting, integrated bonding, and magnetization. The specific preparation process is shown in Figure 2-2(b).

Step 1: Draw the model diagram with 3D modeling software. In order to ensure that the mold surface is smooth and the material is easy to process, polytetrafluoroethylene material is used and processed by a milling machine. The assembly mold uses resin material and is processed by 3D printing technology.

Step 2: Use a precision electronic balance to weigh NdFeB, PDMS, and PDMS curing agent in a mass ratio of 7.5:2:0.5, respectively, then put the weighed NdFeB and PDMS materials into a container, mix and stir thoroughly, then add the weighed PDMS curing agent, mix and put into a vibration mixing instrument, and vibrate for 10 minutes to make the NdFeB more evenly dispersed in the composite

solution. After the vibration is completed, the solution is put into a vacuum chamber for degassing treatment for 10 minutes to completely remove the air bubbles in the solution. Figure 2-3(a) shows the SEM image of the magneto-elastic film obtained after being solidified after being vibrated by the mixing instrument for 10 minutes. It can be seen that the magnetic material is evenly distributed in the film.

Step 3: After removing the bubbles, pour the solution into the mold, spread it evenly, and place it back into the vacuum drying oven, heat it at a constant temperature of 60 ° C for 6 hours to solidify the composite solution. After it is completely solidified, demold and take out the composite material to obtain a magneto-elastic film. Then, use a laser cutting machine to cut out the front fins and rear fins according to the designed shape and dimensions.

Step 4: Put the front fins into the magnetizing machine (Figure 2-3(c)), set the magnetizing voltage to 1700v, and keep it for 10 minutes for magnetization. The magnetization direction is shown in Figure 2-3(b). After magnetization, the robot needs to be integrated and bonded. Put the robot body, front fins, and rear fins into the assembly mold, thinly coat a layer of PDMS solution at the connection, and put it into the vacuum drying oven again, and keep it at a constant temperature of 40° C for 8 hours.

At this point, the design and manufacture of the

bionic cownose ray micro-soft robot is completed. Its structure is similar to that of the real underwater

cownose ray, providing a good model foundation for subsequent experiments.

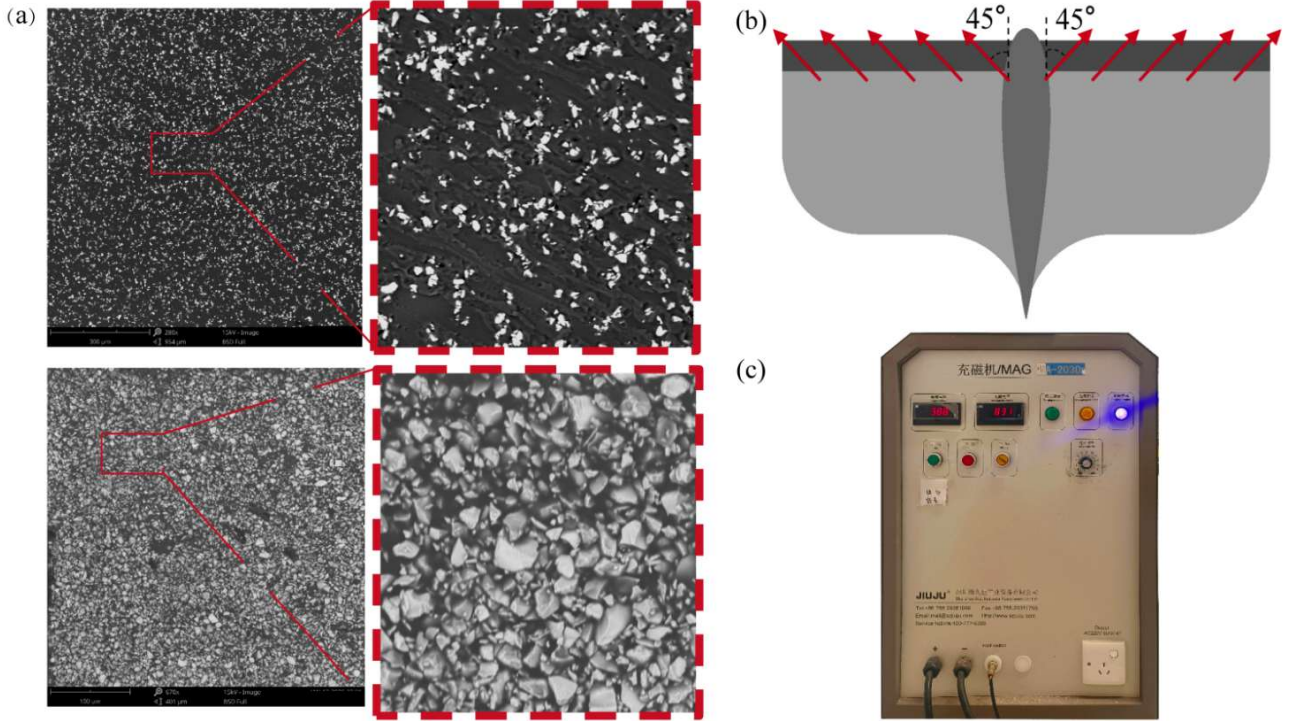


Figure 2-3 (a) SEM images of magneto-elastic films with 50 wt% and 75 wt% NdFeB concentrations, (b) magnetization direction of the robot, (c) magnetizing machine.

3 Driving Mechanism a Micro Soft Robot Mimicking the cownose ray

3.1 Driving Principle a Micro Soft Robot

Mimicking the cownose ray

The cownose soft robot mimicking the cownose ray is driven by an oscillating harmonic magnetic field. When a sinusoidal current signal is input into a single-axis coil, a harmonic magnetic field is generated. Input of a stable current signal into another single-axis generates a uniform magnetic field. On the basis of the harmonic magnetic field, superimposing a uniform magnetic field results in an oscillating harmonic magnetic field. Here, a spatial rectangular coordinate system is established with O-XYZ, with OXY as the planar coordinate system, and the Z-axis as the vertical upward coordinate axis. The oscillating harmonic magnetic field is formed by coupling the harmonic magnetic field B_z along the Z-axis and the uniform magnetic field B_{x-y} in the X-Y plane, as shown in Figure 3-1 (a). The pitch angle α is the angle

between the oscillating harmonic magnetic field B and the OXY plane, and the yaw angle γ is the angle between the projection of the oscillating harmonic magnetic field B on the OXY plane and the X-axis, i.e., the angle between the uniform magnetic field B_{x-y} and the X-axis. In the oscillating harmonic magnetic field, the magnetized magnetic body will be subjected to the magnetic force F and the magnetic torque T , expressed as [37, 38]:

$$F = V(\mathbf{M} \cdot \nabla) \mathbf{B} \quad (2-1)$$

$$\tau = V \mathbf{M} \times \mathbf{B} \quad (2-2)$$

in this equation, V represents the volume of the magnet, \mathbf{M} represents the magnetization intensity of the magnetized magnet, and \mathbf{B} represents the magnetic induction intensity of the external magnetic field generated by the coil, and ∇ represents the gradient operator of the magnetic field. Under the influence of the external magnetic force F , the magnetic medium tends to move towards areas where magnetic field lines are dense. The magnitude of the magnetic force it

experiences is proportional to the gradient of the magnetic induction intensity, and the direction is consistent with the direction of the magnetic induction intensity gradient. When the direction of the magnetic moment of the magnetic medium is not parallel to the direction of the external magnetic field, the magnetic medium will experience a magnetic torque, which will cause it to align its magnetic moment with the direction of the external magnetic field. Therefore, after experiencing the magnetic torque, the magnetic medium will rotate until its magnetic moment aligns with the direction of the external magnetic field. To achieve cable-free magnetic-driven motion of the bio-inspired cownose ray robot, the robot's front fins need to be magnetized, aligning the magnetic moments within the material as illustrated. Under the influence of the oscillating harmonic magnetic field during swinging, the magnetized front fins will experience a magnetic torque. When the front fins swing due to the torque, their movement will also cause the rear fins to swing, resulting in a noticeable bending deformation of the pectoral fins, as shown in Figure 3-1(b). Additionally, since the rear fins cannot directly respond to the magnetic field signals, there is a time lag in the swinging behavior between the front and rear fins, known as phase delay. Figure 3-1(c) presents the force analysis of the bending deformation occurring in the robot's front pectoral fins in the Y-Z plane.

During the robot's movement, the torso experiences almost no deformation, and the propulsion force required for movement mainly comes from the waveforms generated by the deformation of the

pectoral fins on both sides, which push the water flow backward, thereby obtaining a reaction force that propels it forward. This swinging phenomenon is similar to the movement of the pectoral fins of a real cownose ray, where the fish fins create a regular tail vortex flow field during the flapping motion. This tail vortex structure is called a reverse Kármán vortex street, and the jet formed by the reverse Kármán vortex street will exert fluid forces on the fish fins, generating thrust. When the biomimetic fish fin membrane completes one cycle of swinging, the micro-robot will travel a distance of Δs . The larger the swing angle β , the larger the reverse Kármán vortex street formed, resulting in a greater force exerted on the water, allowing it to swim further. Figure 3-1(d) visually demonstrates the three-dimensional shape of the pectoral fin at a certain moment t in the aforementioned kinematic model $Z(x,y,z)$. It clearly reflects the superposition effect of the oscillation component zf and the swinging component zs , which are the gradually decaying oscillation along the chord direction and the swinging motion in the y-z plane with the y-axis as the base axis. The amplitude of the oscillation is largest at the edge of the pectoral fin near the robot's head, with the amplitude gradually increasing along the span direction and decreasing along the chord direction. The periodic fluctuations along the chord direction (X-axis) and the gradually increasing wave amplitude along the span direction (Y-axis) are consistent with the movement characteristics of biological cownose rays.

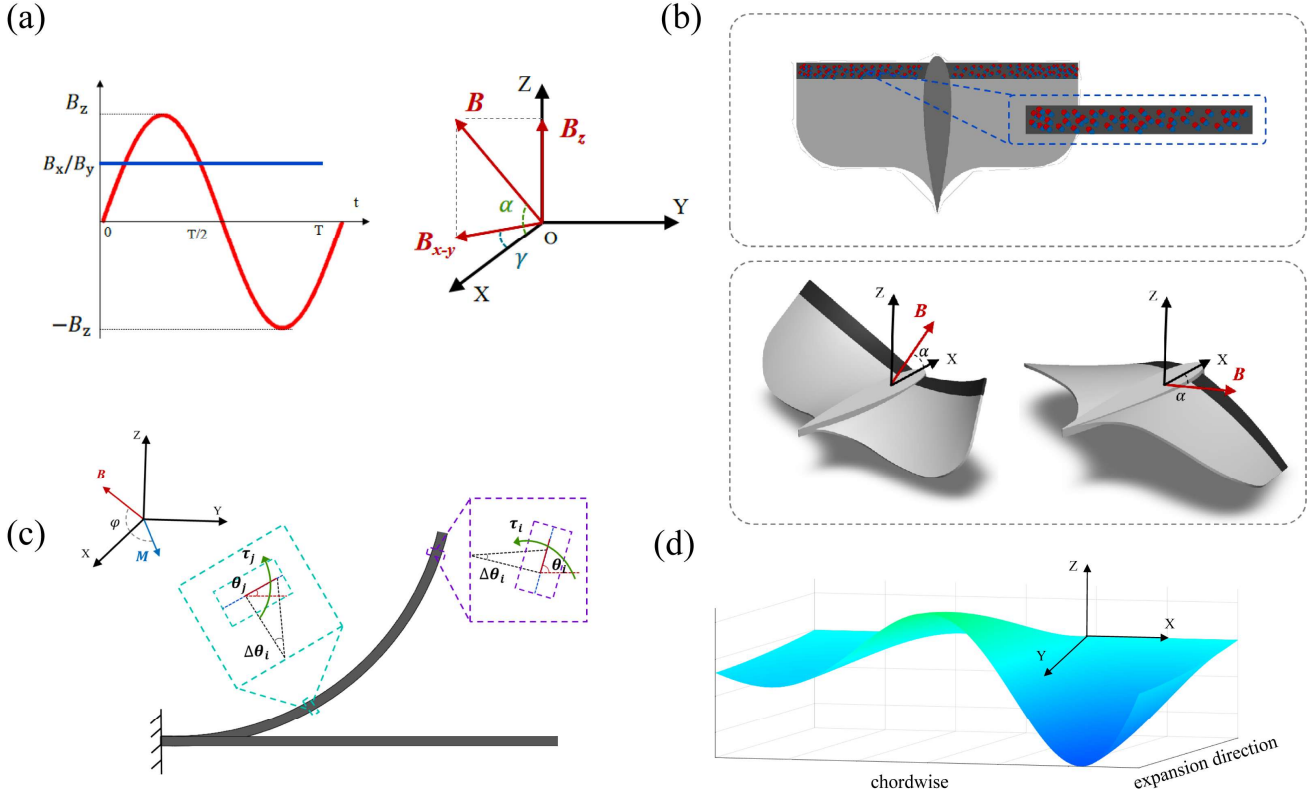


Figure 3-1 (a) diagram of an oscillating harmonic magnetic field, (b) magnetic moment orientation of the anterior fin and Bending deformation of the anterior fin under magnetic torque, (c) front fin bending force deformation analysis diagram, (d) schematic of robot pectoral fin swing.

3.2 Driving System of a Micro Soft Robot

Mimicking the cow鼻 ray

To more precisely control the posture and movement of the robot, we have built a driving system that can generate oscillating harmonic magnetic fields. This biomimetic micro-robot's magnetic field operating system is built on a Helmholtz coil magnetic field platform. The system consists of three orthogonally arranged pairs of Helmholtz coils, which can generate a vector-controllable uniform magnetic field within a specific area of three-dimensional space. The operating principle of the entire magnetic field control system is shown in Figure 3-2(a)(b). This magnetic field driving system includes a control module, a visual feedback module, and the Helmholtz

coils. The Helmholtz coils are the core component of this magnetic field drive system, capable of producing a uniform magnetic field in any direction and size within the working space. To ensure precise motion control of the micro soft robot and provide sufficient magnetic field strength, the wire diameter of the copper wire in the X, Y, and Z axis coils is designed to be 1.2 mm, with the number of turns being 900, 648, and 480 respectively. The inner diameters are 345 mm, 255 mm, and 176 mm, and the outer diameters are 415 mm, 305 mm, and 224 mm, with coil impedances of 14.38Ω , 7.83Ω , and 4.23Ω respectively. The three-axis Helmholtz coils mentioned in this paper were processed by Hunan Yangyi Technology Co., Ltd., with the physical object shown in Figure 3-2(c) and coil parameters listed in table 3-1.

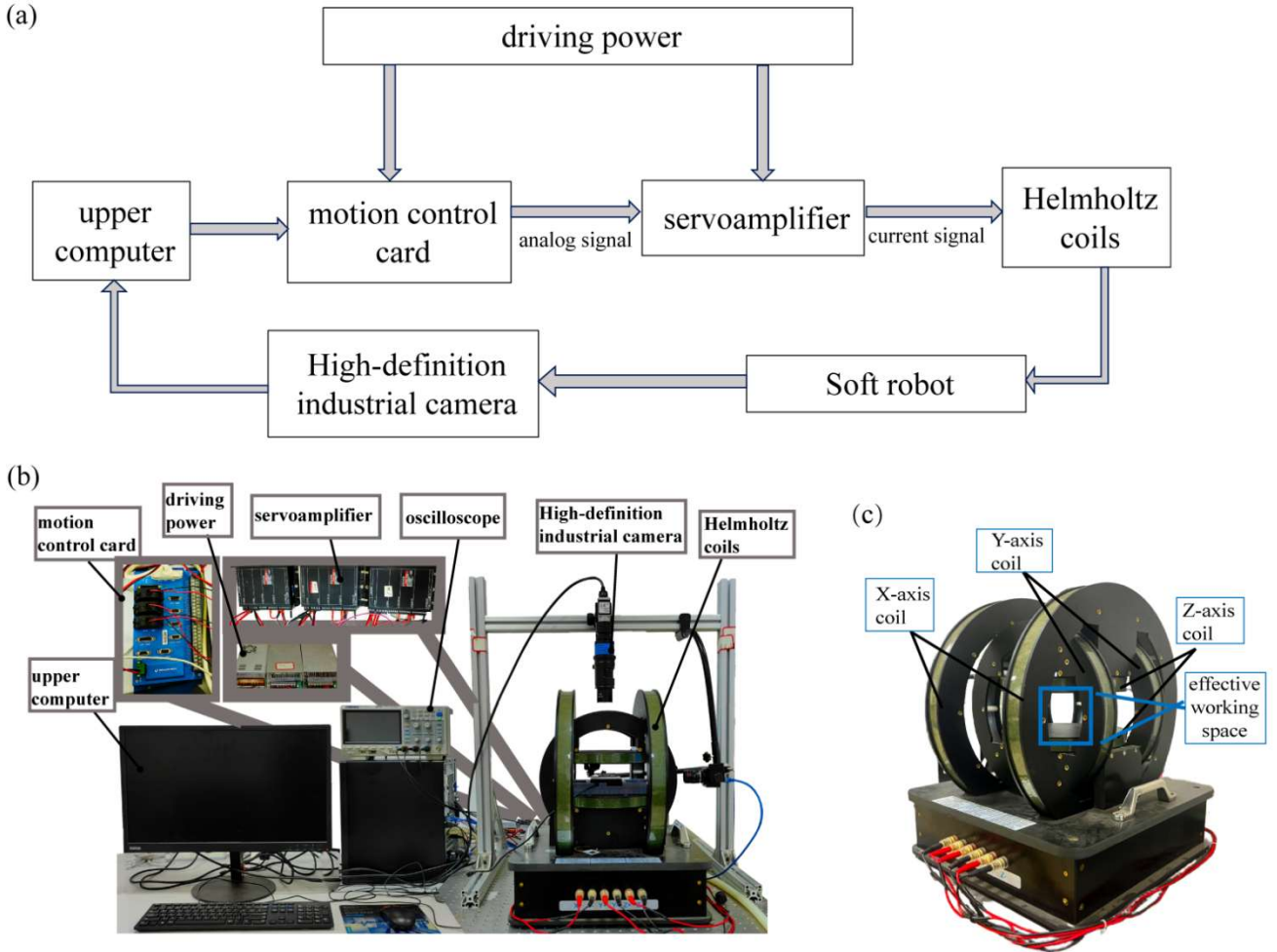


Figure 3-2 (a) magnetic field drive system structure diagram, (b) magnetic field drive test platform, (c) physical diagram of three-dimensional Helmholtz coil.

Table 3-1 helmholtz coil parameters

Coil	Coil	Outer	Inner	Effective	
	Turns	Resistance(Ω)	Diameter(mm)	Diameter(mm)	Radius(mm)
X-axis Coil	900	14.38	418	324	190
Y-axis Coil	648	7.83	310	230	140
Z-axis Coil	480	4.23	224	140	100

In practical applications, the magnetic field strength generated by the electromagnetic coils may deviate, leading to some error in the magnetic field drive system. To ensure precision in the motion control of micro soft robots, this paper uses a teslameter to examine the uniform magnetic field space of the electromagnetic coils. When the Helmholtz coil's uniform magnetic field error is 1%, 2%, and 5%, the

effective working spaces for the X, Y, and Z axes are $42 \text{ mm} \times 60 \text{ mm} \times 80 \text{ mm}$, $51 \text{ mm} \times 71 \text{ mm} \times 96 \text{ mm}$, and $63 \text{ mm} \times 88 \text{ mm} \times 119 \text{ mm}$, respectively. Subsequent experiments will be conducted within a 1% error range.

4 Experiments and Analysis of the Bio-inspired cownose ray Micro Soft Robot

This experiment was conducted within the working range of a three-dimensional Helmholtz coil. By inputting a specific current signal, a required magnetic field is generated to drive the robot's movement. Specifically, we conducted experiments on the straight-line, turning, and directional movements of the bionic cownose ray micro soft robot. The robot was placed in a water-filled container, which was then positioned inside the Helmholtz coil. By inputting

current signals to generate an oscillating harmonic magnetic field, the robot could swim straight, as shown in Figure 4-1(a). From the robot's driving principle, the swimming speed of the cownose ray micro soft robot primarily depends on the oscillation amplitude and frequency of its pectoral fins, which are controlled by the magnetic field strength and signal frequency. To further analyze the influence of these factors on deformation, we analyzed the impact of increasing magnetic field strength and frequency on the deformation angle of the robot's pectoral fins, as shown in Figure 4-1(b). When the frequency (f) is constant at 1 Hz, the greater the sinusoidal magnetic field strength, the larger the deformation angle of the pectoral fins, and the greater the propulsive force the robot receives. When the magnetic field strength is constant, as the magnetic field frequency increases, the bending angle of the pectoral fins decreases. However, this doesn't necessarily mean the robot's swimming speed will decrease. Because as frequency increases, although the propulsive force the robot receives from the fluid decreases in a single cycle, the pectoral fins can oscillate and propel more times within the same cycle. Therefore, increasing the frequency may

accelerate the robot's swimming, but its swimming may slow down when the frequency exceeds a certain value.

To explore the impact of magnetic field strength and frequency on the robot's swimming speed, we tested its swimming performance at frequencies of 1 Hz, 3 Hz, 5 Hz, 7 Hz, 11 Hz, 13 Hz, and 15 Hz, and magnetic strengths of 1.5 mT, 2.25 mT, 3 mT, 4 mT, and 5 mT. As shown in Figure 4-1(c), the micro soft robot performs best in swimming under a magnetic field strength of 5 mT and a frequency of 11 Hz, achieving a maximum swimming speed of 5.25 mm/s. Under the same magnetic field strength, the swimming speed of the robot increases with the frequency, but after exceeding 11 Hz, the swimming speed shows a downward trend. This is because, when the frequency increases to a certain level, if the external magnetic field direction changes, the robot's front fins cannot respond in time and do not achieve maximum bending deformation before the external magnetic field direction changes, greatly affecting the robot's swimming performance. In the research of magnetic-driven robots, this frequency is generally referred to as the "cutoff frequency".

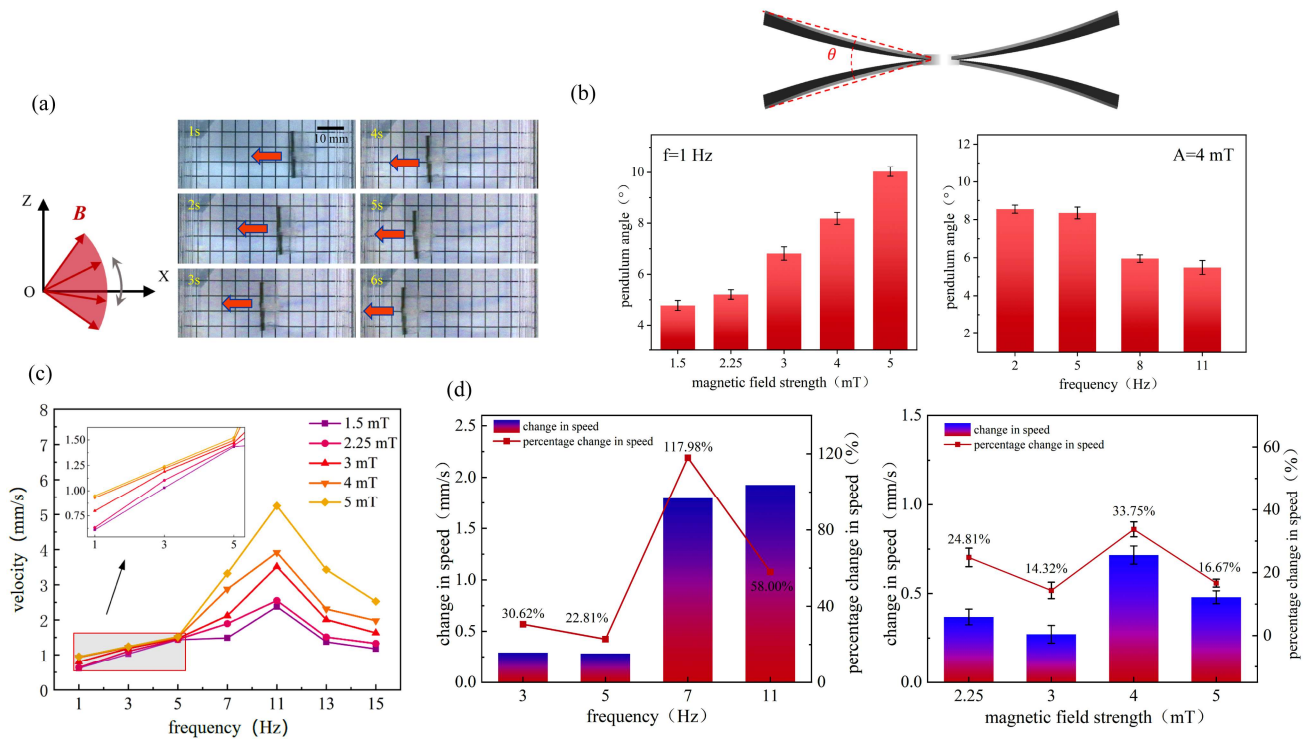


Figure 4-1 (a) shows the robot swimming straight under the magnetic field signal, (b) the relationships of winging angle of the robot's

pectoral fins between magnetic field strength and frequency, (c) shows the swimming speed under different magnetic field strength and frequencies, (d) shows the effect of frequency and magnetic field strength on motion speed.

When the magnetic field frequency remains unchanged, the robot's swimming performance is positively correlated with the magnetic field strength, meaning that the swimming speed increases with the increase of sine magnetic field strength. From the swimming mechanism of the robot, it can be concluded that the greater the magnetic field strength, the greater the magnetic torque experienced, which means a greater degree of bending deformation of the pectoral fins, resulting in greater propulsion force for the robot and thus increased swimming speed. Additionally, from the speed variation curve in Figure 4-1(d), it can be seen that changes in frequency have a more significant impact than changes in magnetic field strength. Using two groups of robots as reference comparisons, we analyzed the changes in swimming speed by varying their sine magnetic field frequency and magnetic field strength. The first group maintained a magnetic field strength of 5 mT, with frequencies of 3 Hz, 5 Hz, 7 Hz, and 11 Hz; the second group maintained a magnetic field frequency of 7 Hz, with magnetic field strengths of 2.25 mT, 3 mT, 4 mT, and 5 mT. As shown in Figure 4-1(d), the line graph indicates the percentage change in the robot's swimming speed, while the bar graph shows the amount of change. From Figure 4-1(d), it can be observed that increasing frequency is more beneficial for the robot's swimming,

especially at high frequencies ($f \geq 7$ Hz), where the change in swimming speed due to frequency variation far exceeds that due to changes in field strength. In low frequencies ($f \leq 5$ Hz), the improvement in swimming performance due to frequency changes is nearly equivalent to that due to changes in field strength. Therefore, as long as the cutoff frequency is not exceeded, increasing the frequency of bending deformation of the pectoral fins is more advantageous for improving the swimming performance of the bio-inspired cownose ray micro soft robot compared to increasing magnetic field strength.

As mentioned earlier, the yaw angle γ is the angle between the uniform magnetic field B_{x-y} and the X-axis, which is the angle between the direction under the combined action of uniform magnetic fields in the X and Y directions and the X-axis. By changing the magnitude and direction of the current in the input coil, the direction of the uniform magnetic field can be changed, thereby changing the robot's direction of movement. Therefore, in the oscillating harmonic magnetic field, changing the direction (yaw angle γ) of the uniform magnetic field on the X-Y plane can change the robot's direction of travel and complete the turning action. At a frequency of $f = 7$ Hz and a magnetic field strength $H = 3$ mT, we explored the robot's turning situations to the right at 30° , 60° , ..

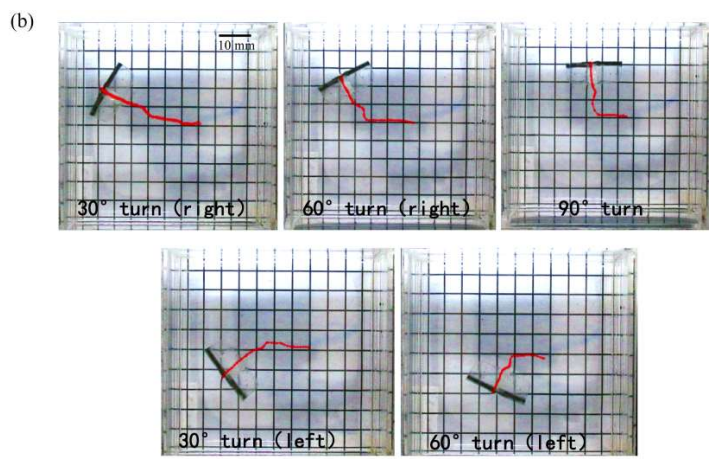
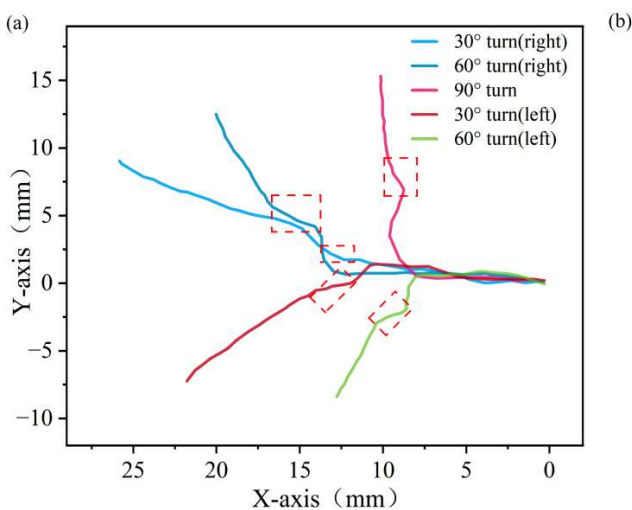


Figure 4-2 (a) the robot's turning swimming deviation, (b) the robot's turning swimming trajectory.

and 90° , and to the left at 30° and 60° , with the robot's motion trajectory shown in Figure 4-2(b). Through experiments, it was found that the robot exhibits two instances of swimming deviation during the response to steering actions, occurring at the beginning and end of the response, as shown in Figure 4-2(a). At the initial stage of the robot's response to the steering action, the steering angle of the robot is greater than the target angle; while at the end of the response, the swimming direction of the robot shows a drifting phenomenon. To explore this phenomenon, the steering movements of the robot were tested under two conditions: increasing magnetic field strength and increasing magnetic field frequency. The first set of Figure 4-3(a), shows the robot completing 30° and 60° turns with a constant magnetic field strength of 5 mT, while the magnetic field frequency changes from 8 Hz to 11 Hz, 14 Hz, and 16 Hz. The second set of Figure 4-3(c) shows the robot completing 30° and 60° turns with a constant magnetic field frequency of 11 Hz, while the magnetic field strength increases from 1.5 mT to 2.25 mT, 3 mT, 4 mT, and 5 mT.

In this motion experiment, the same pattern of motion deviation can be observed, occurring twice, as highlighted in boxes in Figure 4-3(b)(d). At the initial stage of the robot's steering response, the robot exhibits a motion trajectory greater than the steering angle (box b), and then, while moving towards the target angle, another drift phenomenon occurs along the original motion direction (X direction) (box a). Subsequently, the robot corrects its swimming direction and moves towards the target direction to complete the turn. The two instances of motion error generated during the robot's steering are referred to in the text as "response error" and "inertia error." When the direction of the external magnetic field signal changes, the robot experiences a corresponding magnetic torque, causing it to align with the direction of the magnetic field signal. However, due to the

sudden change in the magnetic field direction over a short period, the steering force acting on the robot suddenly increases, resulting in the robot's steering exceeding the target angle. Once the magnetic field signal stabilizes, the robot will correct its direction and swim towards the target angle. This error phenomenon is termed "response error offset". When the robot continues to swim towards the target angle, a second motion drift occurs, this time due to inertial forces. After completing the steering response action, the robot immediately changes its motion posture to swim towards the target angle, during which the presence of the robot's own inertial force alters its motion direction. The direction of the inertial force generally aligns with the motion direction prior to the steering action, which in this experiment is along the X-axis. This motion drift phenomenon caused by inertial forces is referred to as "inertia error drift." In fact, "inertia error" does not only occur at the end of the steering but is coupled with "response error" from the initial stage of the steering response, jointly leading to the motion deviation phenomenon at the beginning (box b). It only manifests independently in the drift trajectory after the "response error" disappears. Furthermore, the magnitude of the "response error" is influenced by the magnetic field strength and the rate of change of the magnetic field direction, while the magnitude of the "inertia error" is primarily influenced by the speed of motion during straight-line movement, which is also affected by the magnetic field strength. Therefore, both types of errors are simultaneously influenced by the strength of the external driving magnetic field. Generally speaking, the greater the magnetic field strength, the shorter the correction time for the robot's motion direction, and the less significant the motion drift. From Figure 4-3(b)(d), it can be seen that during the robot's completion of 30° and 60° turns, the motion trajectory drift error shows a decreasing trend with increasing magnetic field strength, and the

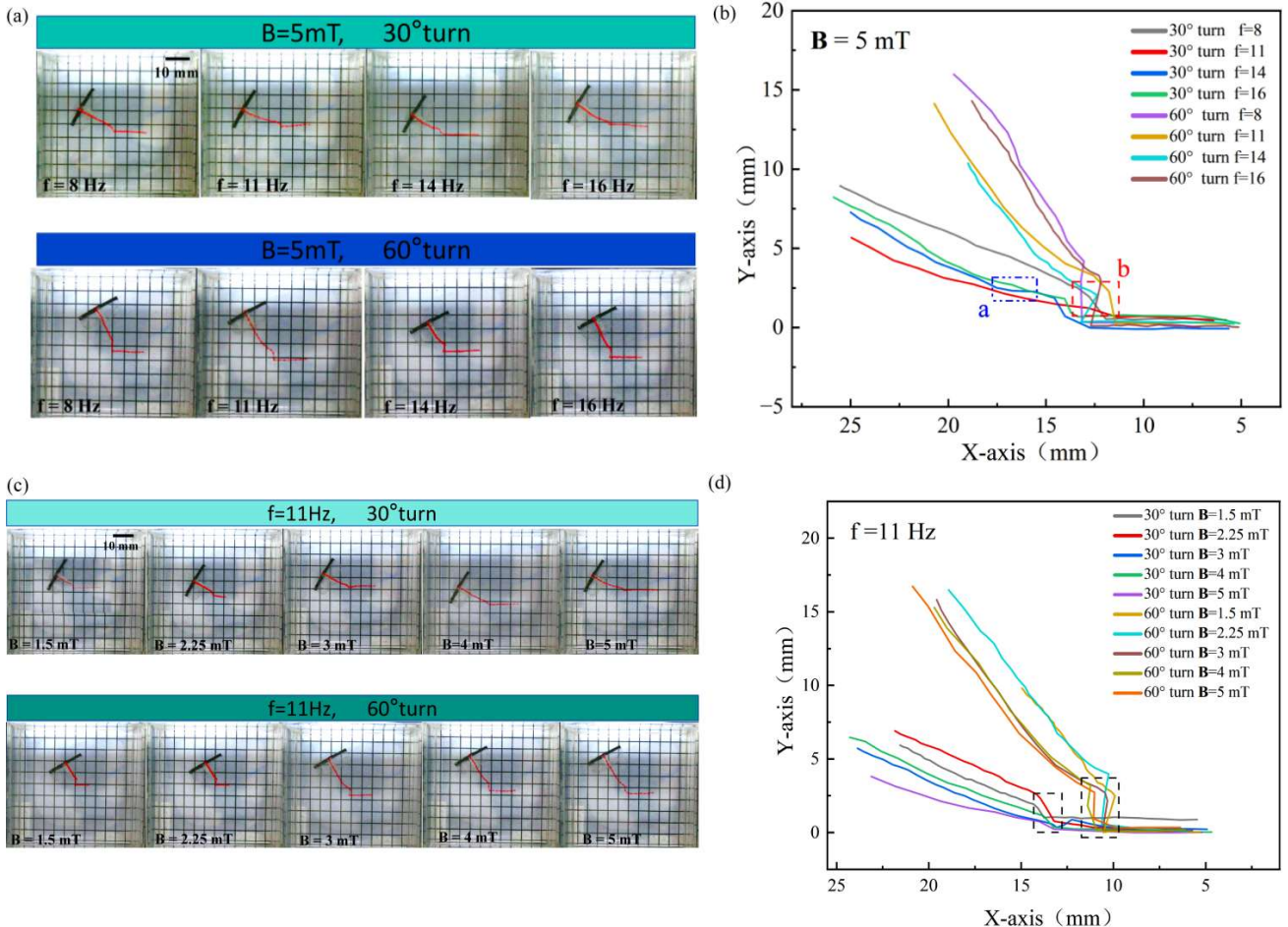


Figure 4-3(a) Figure (a) The robot's steering movement at different frequencies with a constant field strength, (b) The robot's steering movement trajectory at different frequencies with a constant field strength, (c) The robot's steering movement at different field strengths with a constant frequency, (d) The robot's steering movement trajectory at different field strengths with a constant frequency. correction time also becomes shorter, meaning the robot completes the steering action more quickly and reaches stability.

To better verify the correlation and degree of association between the yaw angle of the magnetic field signal and the swimming direction of the robot, we conducted experiments by changing the yaw angle to drive the robot to complete three trajectory experiments: "Z", "□", and "∇". In this experiment, the relevant magnetic field parameters were: oscillating harmonic magnetic field frequency $f = 11$ Hz, magnetic field strength $B = 4$ mT, and the pitch angle α was 45° . In the "Z" trajectory, the magnetic field parameters were kept constant, with yaw angles γ of 0° , -45° , and 0° ; in the "□" trajectory, γ was 0° , -45° , -90° , -135° , -180° , 135° , and 90° ; in the "∇" trajectory, γ was -45° , 75° , and -165° . Figure 4-4(a)

shows the directional swimming trajectory of the robot, where it can be observed that the robot's trajectory is highly consistent with the target trajectory, indicating that the robot has superior directional movement performance, while also verifying the correlation between the robot's swimming direction and the yaw angle γ . From the mechanism of robot movement, it can be seen that the steering action is caused by changes in the direction of the magnetic field. When there is a sudden change in the magnetic field direction, the robot's movement inertia can lead to a phenomenon of motion deviation. In this instance, the robot also exhibited motion deviation while completing the directed swimming action. As shown in Figure 4-4(b), different degrees of motion deviation occurred in the experiments with the "Z", "□", and "∇" trajectories. Among them, the deviation error for the "□" trajectory

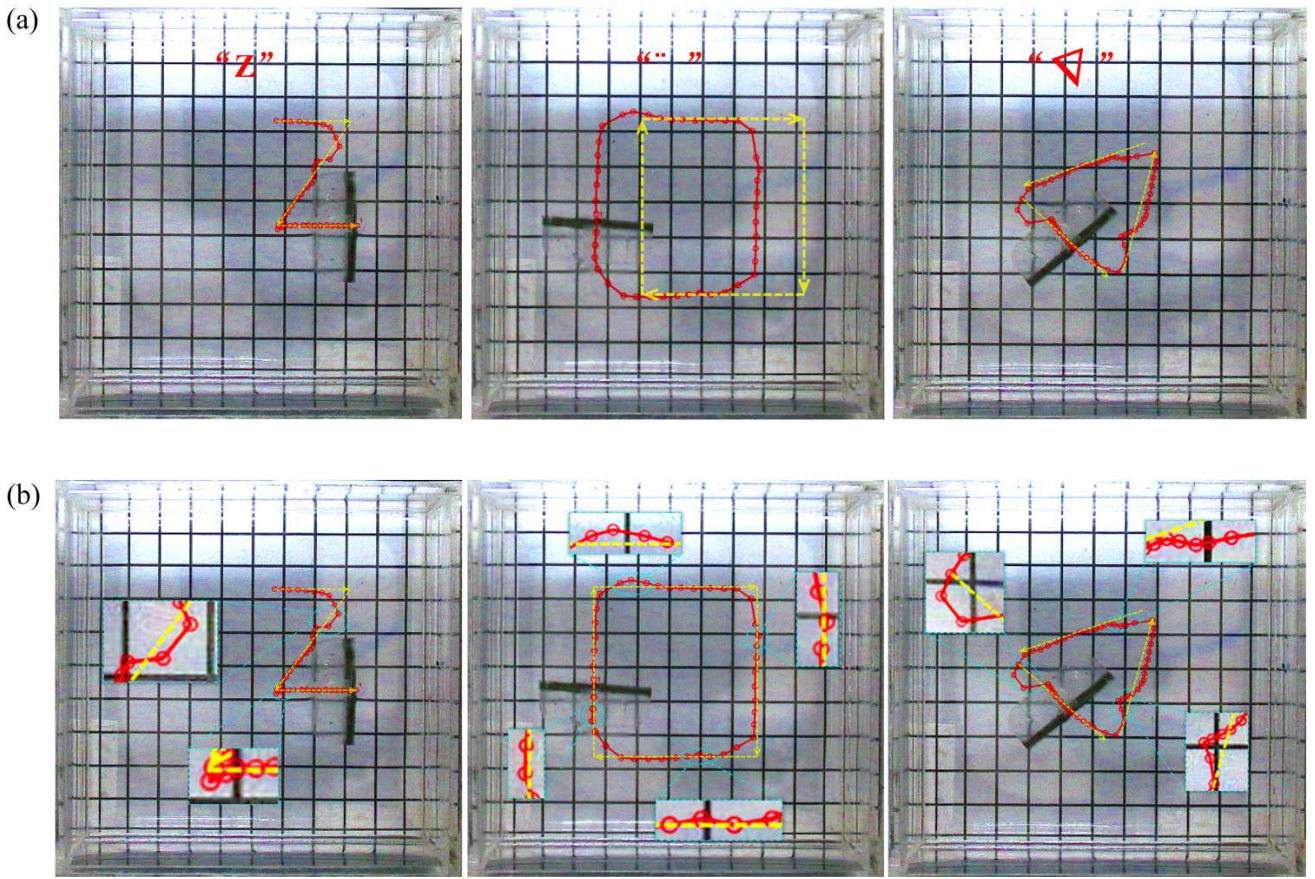


Figure 4-4 (a) robot directional path swimming, (b) directional path swimming deviation error phenomenon.

was the smallest, while the deviation error for the "V" trajectory was the largest. This is because only the "□" trajectory experiment employed a steering decomposition approach, which breaks down a single steering action into two steering actions, significantly reducing the motion deviation caused by "response error." The other two trajectory experiments did not use decomposition, resulting in more noticeable motion deviations, particularly in the "V". This is because the single steering angle for the "V" trajectory is 60° , while the single steering angle for the "Z" trajectory is 45° . It can be seen that the larger the single steering angle, the more severe the resulting motion deviation will be. The "inertia error" is mainly determined by the robot's movement speed, and this error can only be reduced by slowing down the robot's swimming speed. However, the "response error" is influenced by both the speed of change in the magnetic field direction and the magnitude of the magnetic field strength. To minimize the "response error," steering

decomposition can be used to complete the steering action.

5 Conclusions

This paper focuses on micro-soft robots, conducting biomimetic design based on the biological characteristics and swimming mechanisms of the cow-nose ray, utilizing magnetic control driving principles. It proposes a design method for magnetic-driven cow-nose ray mimetic micro-soft robots and proves their reliable swimming capability. The robot is fabricated using a certain proportion of NdFeB, PDMS, and curing agents. By utilizing Helmholtz coils to generate oscillating harmonic magnetic fields, the robot achieves straight-line swimming, turning, and specific path swimming. Experimental results show that the swimming speed is fastest at $B = 5$ mT and $f = 11$ Hz, reaching 5.25 mm/s, approximately 0.5 body lengths per second. Additionally, experimental comparisons reveal that the robot's motion performance is limited by the cutoff

frequency, and exceeding this frequency results in a decrease in swimming speed. During experiments, adjusting the yaw angle γ allows for precise control of the swimming direction of the cow-nose ray mimetic soft robot, achieving turning and directional path swimming. During the robot's swimming process, "response errors" and "inertial errors" exist. By adjusting the yaw angle γ in steps, the influence of "response errors" on the motion trajectory can be effectively reduced. These experiments lay an important foundation for the study of tether-free control of underwater micro-soft robots. Furthermore, this research provides important references for the fields of biomimetic robots and magnetically controlled micro-soft robots. Future work will focus on refining the precise control of motion performance and exploring the impact of multi-physical field control on robot motion performance.

Acknowledgments This work is supported by the Guangzhou Science and Technology Plan Project (No. SL2024A03J00589). These supports are gratefully acknowledged.

Data Availability The datasets generated during and analyzed during the current study are available from the corresponding author on reasonable request.

Declarations

Conflict of Interest There are no conflicts to declare.

6 References

- [1] Wissem H ,Michaël G ,Kanty R .Miniaturized Soft Robotics: Recent Advances and Future s Opportunities[J].Current Robotics Report s, 2024, 5 (2) :15–27. DOI:10.1007/S43154-024-0 0109-3.
- [2] Kabutz H ,Jayaram K .Design of CLARI: A Mi niature Modular Origami Passive Shape - Mor phing Robot[J].Advanced Intelligent System s, 2023, 5 (12) :DOI:10.1002/AISY.202370057.
- [3] Fuller S B. Four Wings: An Insect-Sized Ae rial Robot With Steering Ability and Paylo ad Capacity for Autonomy[J]. Ieee Robotics and Automation Letters, 2019, 4 (2):570–57 7.
- [4] Wang C Y, Zhang W P, Zou Y, et al. A Sub-1 00 mg Electromagnetically Driven Insect-in spired Flapping-wing Micro Robot Capable o f Liftoff and Control Torques Modulation [J]. Journal of Bionic Engineering, 2020, 17 (6) :1085–1095.
- [5] ZhuK ,LiH ,ZhaoW , et al. A Millimeter - Sca le Micro Crawling Robot with Fast - Moving Driven by a Miniature Electromagnetic Line ar Actuator[J]. Advanced Intelligent System s, 2024, 6 (8) :2300909–2300909. DOI:10.1002/AI SY.202300909.
- [6] Xiong Q, Zhou X, Li D, et al. An Amphibiou s Fully - Soft Centimeter - Scale Miniature Crawling Robot Powered by Electrohydraulic Fluid Kinetic Energy [J]. Advanced Scienc e, 2024, 11 (14).
- [7] Wang C, Li H Z, Zhang Z Z, et al. Review o f Bionic Crawling Micro-Robots[J]. Journal of Intelligent & Robotic Systems, 2022, 1 05 (3) :17.
- [8] Chang J, Song Q, Li R, et al. Design and M otion Characteristics of a Ray-Inspired Mi cro-Robot Made of Magnetic Film [J]. Journ al of Bionic Engineering, 2024, 21 (6) : 274 5 – 2758.
- [9] Teng X, Qiao Z, Yu S, et al. Recent Advanc es in Microrobots Powered by Multi-Physics Field for Biomedical and Environmental Ap plications [J]. Micromachines, 2024, 15 (4) : 492.
- [10] Zhu B, Wang Y Q. Fast - Moving and Highly A daptable Hollow Piezoelectric Miniature Ro bot [J]. Advanced Intelligent Systems, 202 4, 6 (4).
- [11] Salazar, R. ; Fuentes, V. ; Abdelkefi, A. Cl assification of biological and bioinspired

aquatic systems: A review. *Ocean. Eng.* 2018, 148, 75–114.

[12] Sfakiotakis, M.; Lane, D.; Davies, J. Review of Fish Swimming Modes for Aquatic Locomotion. *IEEE J. Ocean. Eng.* 1999, 24, 237–252.

[13] Wu J, Wu G, Guo Y, et al. Overall design and flutter motion analysis of a semi-active manta ray robot[C]// OCEANS 2019 MTS/IEEE SEATTLE. Seattle, WA: IEEE, 2019: 1–6.

[14] Teng X, Qiao Z, Yu S, et al. Recent Advances in Microrobots Powered by Multi-Physics Field for Biomedical and Environmental Applications [J]. *Micromachines*, 2024, 15(4): 492.

[15] Chu Y, Wang X, Hao T, et al. Design and Performance Study of a Six-Bar Mechanism Underwater Robot Based on Cownose Ray Bionics [J]. *Journal of Marine Science and Engineering*, 2025, 13(6): 1156–1156. DOI:10.3390/JMSE13061156.

[16] Zhang D, Pan G, Cao Y, et al. A novel integrated gliding and flapping propulsion biomimetic manta-ray robot[J]. *Journal of Marine Science and Engineering*, 2022, 10(7): 924.

[17] Giovanni B, Lorenzo M, Michele T, et al. A Bioinspired Cownose Ray Robot for Seabed Exploration. [J]. *Biomimetics* (Basel, Switzerland), 2023, 8(1): 30–30. DOI:10.3390/BIOMIMETICS8010030.

[18] Xu Z, Liang J, Zhou Y, et al. Manta ray-inspired soft robotic swimmer for high-speed and multi-modal swimming[C]// 2024 IEEE/RSJ International Conference on Intelligent Robots and Systems (IROS). New York: IEEE, 2024: 235–240.

[19] Li T, Li G, Liang Y, et al. Fast-moving soft electronic fish[J]. *Science advances*, 2017, 3(4): 1602045.

[20] Yin C, Wei F A, Fu S H, et al. Visible light-driven jellyfish-like miniature swimmin

g soft robot[J]. *Acs Applied Materials & Interfaces*, 2021, 13(39): 47147–47154.

[21] Gao Y, Wei F, Chao Y, et al. Bioinspired soft microrobots actuated by magnetic field [J]. *Biomedical Microdevices*, 2021, 23: 1–19.

[22] Xu H, Bai S, Gu G, et al. Bioinspired self-resettable hydrogel actuators powered by a chemical fuel[J]. *Acs Applied Materials & Interfaces*, 2022, 14(38): 43825–43832.

[23] Akolpoglu M B, Alapan Y, Dogan N O, et al. Magnetically steerable bacterial microrobots moving in 3D biological matrices for stimuli-responsive cargo delivery[J]. *Science Advances*, 2022, 8(28): 6163.

[24] Ilami M, Bagheri H, Ahmed R, et al. Materials, actuators, and sensors for soft bioinspired robots[J]. *Advanced Materials*, 2021, 33(19): 2003139.

[25] Jeon S, Hoshiar A K, Kim K, et al. A magnetically controlled soft microrobot steering a guidewire in a three-dimensional phantom vascular network[J]. *Soft Robotics*, 2019, 6(1): 54–68.

[26] Schuerle S, Erni S, Flink M, et al. Three-dimensional magnetic manipulation of micro- and nanostructures for applications in life sciences[J]. *IEEE Transactions on Magnetics*, 2013, 49(1): 321–330.

[27] Thornley C R, Pham L N, Abbott J J. Considering six-degree-of-freedom magnetic actuation across scales[J]. *Ieee Robotics and Automation Letters*, 2019, 4(3): 2325–2332.

[28] Fan Q, Zhang P, Qu J, et al. Dynamic magnetic field generation with high accuracy modeling applied to magnetic robots[J]. *IEEE Transactions on Magnetics*, 2021, 57(7): 1–10.

[29] Mahoney A W, Abbott J J. Generating rotating magnetic fields with a single permanent magnet for propulsion of untethered magne

tic devices in a lumen[J]. IEEE Transactions on Robotics, 2014, 30(2): 411-420.

[30] Popek K M, Hermans T, Abbott J J. First demonstration of simultaneous localization and propulsion of a magnetic capsule in a lumen using a single rotating magnet[C]// 2017 IEEE International Conference on Robotics and Automation (ICRA). Singapore: IEEE, 2017: 1154-1160.

[31] Ryan P, Diller E. Magnetic actuation for full dexterity microrobotic control using rotating permanent magnets[J]. IEEE Transactions on Robotics, 2017, 33(6): 1398-1409.

[32] Shamsudhin N, Zverev V I, Keller H, et al. Magnetically guided capsule endoscopy[J]. 2017, 44(8): 91-111.

[33] Hu W, Lum G Z, Mastrangeli M, et al. Small-scale soft-bodied robot with multimodal locomotion[J]. Nature, 2018, 554(7690): 81-85.

[34] Huang C, Lai Z, Zhang L, et al. A magnetically controlled soft miniature robotic fish with a flexible skeleton inspired by zebrafish[J]. Bioinspiration & Biomimetics, 2021, 16(6): 065004.

[35] Venkiteswaran K V , Samaniego P F L , Sikorski J , et al. Bio-Inspired Terrestrial Motions of Magnetic Soft Millirobots. [J]. IEEE Robotics and Automation Letters, 2019, 4(2):1753-1759.

[36] Yang, S. B. Kinematic analysis of cow-nosed ray swimming and research on bionic robotic fish [Master's thesis, National University of Defense Technology, 2010]. Changsha City, China.

[37] Liu, C. S., The g-based Jordan algebra and Lie algebra formulations of the Maxwell equations[J]. Journal of Mechanics, 2004. 20(4): p. 285-296.

[38] Kim, Yoonho, Xuanhe Zhao, Magnetic Soft Materials and Robots[J]. Chemical Reviews, 2022. 122(5): p. 5317-5364.